Correcting land surface temperature measurements for directional emissivity over 3-D structured vegetation

Yunyue Yu*[a], Ana C. Pinheiro[b], Jeffrey L. Privette[c]
[a]Earth Systems and Geoinformation Sciences, George Mason University, USA;
[b]National Research Council Postdoctoral Associate, USA;
[c]NASA's Goddard Space Flight Center, USA
*yunyue.yu@gsfc.nasa.gov; phone 1 301 614-6494; fax 1 301 614-6695

ABSTRACT

The emissivity variation of the land surface is the most difficult effect to correct for when retrieving land surface temperature (LST) from satellite measurements. This is not only because of the emissivity inter-pixel variability, but also because each individual pixel is a combination of different surface types with different emissivies. For different illumination-observation geometries, this heterogeneity leads to different ensemble (scene) emissivities. The modified geometric project (MGP) model has been demonstrated to be able to simulate such effect when the surface structural characteristics are available. In this study, we built a lookup table to correct the surface emissivity variation effect in LST retrievals. The lookup table is calculated using the MGP model and the MODTRAN radiative transfer model. The MGP model, assumes that the land surface visible to the satellite sensor is a composite of homogeneous vegetation and soil background surface types. The homogeneous or "pure" surface types and their emissivity values are adopted from Snyder's surface type classification. Our simulation procedure was designed to calculate the emissivity directional variation for multiple scenarios with different surface types, solar-view angles, tree cover fractions, and leaf area index. Analysis of the MODTRAN simulation results indicates that an error of over 1.4 K can be observed in the retrieved LST if surface emissivity directional variability is not accounted for. Several MODIS granule data were selected to evaluate the correction method. The results are compared with the current MODIS LST products.

Keywords: land surface temperature, LST algorithm, satellite remote sensing, emissivity, directional effects

1. INTRODUCTION

It is well known that the knowledge of land surface temperature (LST) over large spatial and temporal scales is of fundamental importance to many applications, such as agrometeorology, climatic and environmental studies. Satellite remote sensing is the only means available to obtain regional and global LST on a synoptic and regular basis. Currently, those sensors such as Advanced Very High Resolution Radiometer (AVHRR) onboard the NOAA polar-orbiting meteorology satellites and the Moderate Resolution Imaging Spectroradiometer (MODIS) onboard the NASA Earth Observation systems (EOS) satellites are the major sources of LST products. In the near future, the visible infrared imaging radiometer suite on board the National Polar-orbiting Operational Environmental Satellite System (NPOESS) will replace the AVHRR and the MODIS as the nation's wide-swath multispectral sensor following the launch of the NPOESS Preparatory Project (NPP) satellite around 2009.

The physics behind the retrievals of LST from space is based on the theory of multiple radiative transfer processes between the surface and the satellite sensor. By linearizing the radiative transfer equations at two adjacent thermal infrared channels, a split-window method was developed and had first been applied for sea surface temperature (SST) retrievals [1]. Applying the split-window method for LST retrievals is however more difficult, mainly because the emissivity of land surface is not close to unity (as is for SST retrieval) and is a function of land surface type. Unfortunately, simulation studies have indicated that most split-window LST algorithms are sensitive to the emissivity variation [2]. Therefore, accurate land surface emissivity information is needed in split-window LST algorithms.

Currently there are basically two measures available to obtain the land surface emissivity information on a global basis. Snyder *et al.* [3] described a surface type-emissivity mapping method, in which each land surface type classified by the International Geosphere-Biosphere Programme (IGBP) was matched to a spectral emissivity value that was

Remote Sensing and Modeling of Ecosystems for Sustainability III, edited by Wei Gao, Susan L. Ustin,
Proc. of SPIE Vol. 6298, 629817, (2006) · 0277-786X/06/$15 · doi: 10.1117/12.682951

experimentally measured. This method is operationally simple yet statistically accurate in the thermal infrared channels for most of the IGBP types. Alternately, Wan *et al.* [3] developed a day-night algorithm that derives LST and surface emissivity simultaneously using multiple channel measurements of the same land surface area for both day and night. The emissivity product is currently available through the MODIS MOD11 product. Emissivity derived from the day-night algorithm is expected to be more accurate than that derived from Snyder's type-emissivity mapping method and account for the temporal variability of this parameter. However, availability of the data from the day-night algorithm is poor because the percentage of the cloud-free cases for the day-night pairs is very small in the total data stream.

Another concern, which is the focus of this study, is that both the methods mentioned above do not have any consideration for the directional dependency of emissivity, meaning that the LST derived using the split-window LST algorithms assumed a Lambertian surface. This may introduce considerable error. Pinheiro *et al*. [5] demonstrated in their AVHRR LST retrieval using the Ulivieri' split-window algorithm [6] that, for a structured vegetation surface, an artificial signal may be introduced in the retrieved LST for different view zenith angles, for structured surfaces where the endmembers display very different temperatures. This directional effect is due to the fact that proportions of canopy and surface 'endmembers' (e.g., sunlit soil, shaded trees) visible to the sensor vary with the view angle, with the result that the ensemble surface emissivities of the two thermal infrared channels vary with the sun-view geometry. Due to the sensitivity of the split-window LST algorithm, the derived LST of the scene can vary with the sun-view geometric direction.

Currently, the above structural emissivity directional variation is not counted in any of the LST algorithms. Instead, a constant emissivity is assumed for all observation geometries. In this paper, we investigated the LST directional changes due to the emissivity directional effect using simulation datasets generated by coupling the modified geometric projection (MGP) model to the MODTRAN radiative transfer model [7]. We developed a directional emissivity lookup table (LUT) using the MGP model, which then can be applied for retrieving directional LST from satellite data. Using the MODTRAN radiative transfer model we model the LST directional effect due to the emissivity directional effect. To test and demonstrate our approach we applied the LUTs to several MODIS scenes.

The outline of this paper is as follows. In the following two sections, we provide details of simulation studies using the MGP model and the MODTRAN radiative transfer model, respectively. The simulation results are presented in Section 4. In Section 5, we apply the emissivity LUTs, that were generated in the simulation study of the MGP model, on the MODIS data for a directional effect corrected LST derivation. The newly derived LSTs are then compared to the MODIS LST product. Discussions of the simulation results and the MODIS data application are given in Section 6. Finally, we present conclusions in Section 7.

2. SIMULATION OF THE MGP MODEL

2.1 Modified geometric projection model

Satellite sensor measures the land surface from pixel to pixel. Each pixel, with a certain resolution, is considered as an entity composed of a variety of endmembers (i.e., surface types). The satellite sensed LST is a representation of the total scene composite of temperatures and is also know as the 'apparent' temperature. The MGP model, used to simulate these scenarios, assumes that 1) the radiance emitted from the composite area is a linear contribution of the radiances emitted by each endmember weighted by its projected fraction and, 2) the endmembers are isotropic emitters. In the model, each endmember is characterized by its temperature T_k, emissivity ε_k, and a fraction cover probability $X_k(\theta, \phi)$, where θ and ϕ represent view zenith angle and relative sun-view azimuth angle, respectively. Assuming that the pixel is composed of N endmembers, the apparent temperature distribution $T(\theta, \phi)$ can be estimated through a linear combination formula, i.e.,

$$< T(\theta,\phi) >= \left[\frac{1}{< \varepsilon(\theta,\phi) >} \sum_{k=1}^{N} \varepsilon_k T_k^4 X_k(\theta,\phi) \right]^{1/4} \tag{1}$$

with $<\varepsilon(\theta,\phi)>$ defined as the weighted mean of endmember emissivity, i.e.,

$$< \varepsilon(\theta,\phi) >= \sum_{k=1}^{N} \varepsilon_k X_k(\theta,\phi) \tag{2}$$

Wavelength is omitted in the above equations, but the sensor central wavelength is implied.

It is important to point out that, although the endmembers are assumed as isotropic emitters, the 'apparent' emissivity $\varepsilon(\theta, \phi)$ and temperature $T(\theta, \phi)$ are sun-view geometric dependent. This is because the projected fraction of each endmember, $X_{k,}$ varies with the sun-view geometry.

The MGP model relies on a geometric optics (GO) modell [8] to calculate the projected fractions $X_k(\theta, \phi)$., and simulates the scene as a set of discontinuing canopies composed of four endmembers: sunlit crow, shaded crown, sunlit background, and shaded background. The GO model represents the surface as a collection of spheroids on vertical sticks. Location of those spheroids follows a Poisson distribution. and Boolean set theory is used to calculate within and between crown gap probabilities. More details of the MGP model can be found in [9].

2.2 Parameters of the MGP model

Running the MGP model requires a variety of input parameters. Table 1 lists those parameters and their values used in this simulation. Among those, the minimum and maximum tree heights, the crown height, diameter and the leaf area index (LAI) are the structural parameters of the canopy; the solar zenith angle, the view zenith angle and the solar-view relative azimuth angle are the solar-view geometric parameters; the temperatures of the four endmembers, and the emissivities of the canopy and the ground are the endmember property parameters. The emissivities for sunlit and shaded endmembers are assumed to be the same.

Table 1. Input parameters for the MGP model simulation

Parameter	Value
Solar zenith angle (degree)	0, 30, 60
View zenith angle (degree)	0, 10, 20, 30, 40, 50 60, 70
Solar-view relative azimuth (degree)	0, 180
Sun lit canopy temperature	T_{surf} + 5
Shade canopy temperature	T_{surf}
Sun lit background temperature	T_{surf} +15
Shade background temperature	T_{surf}
Canopy emissivity	In a range from 0.9650, 0.9911
Ground emissivity	In a range from 0.9400 to 0.9820
Tree cover fraction (%)	10, 20, 30, 40, 50, 60, 70, 80, 90
Minimum tree height	5
Maximum tree height	15
Canopy crown height	5
Canopy crown diameter	2
Leaf area index	0.2, 0.4, 0.6, 0.8, 1, 2, 3, 4, 5

Note that, in Table 1, we used a variety range of values for different parameters except the tree structural parameters. Pinheiro *et al*. [9] showed that LST directional retrievals are most sensitive to observation-illumination geometry and tree cover fraction; other structural factors (e.g., tree height, canopy width, etc) are less relevant in studying this process. In this study, we performed tests using different combinations of the tree structural parameters with a fixed set of the geometric and property parameters. The difference of the output emissivities for those scenarios is irrelevant. Therefore, in our simulation analysis, we used a fixed value set for the minimum and maximum tree heights, the crown height, and the diameter. Temperatures of the endmembers were also fixed since we are more interested in the apparent surface emissivity change than the surface temperature change.

2.3 Directional emissivity lookup table

A lookup table of the directional emissivity can be generated using the above input combinations into the MGP model. Note that only the emissivities of the input parameters are wavelength dependent. By using different set of spectral values of the canopy emissivity and the ground emissivty, the directional emissivity LUT represents different sensor channels. In this study, we simulated the data for the MODIS bands 31 and 32, with the wavelength centered at 11.030 μm and 12.020 μm, respectively.

Six spectral emissivity values were adapted from Snyder *et al*.'s emissivity classification study [3], representing four tree cover types and two background types, respectively. The tree cover types are the evergreen needle leaf forest, the

evergreen broad leaf forest, the deciduous needle leaf forest and the deciduous broad leaf forest; the ground types are the organic bare soil and the herbaceous. Emissivity value of the tree cover types was applied directly as the canopy emissivity (Table 1), while the background emissivity value was proportionally combined from the emissivities of soil ground and the herbaceous, i.e.,

$$\varepsilon_g = \frac{a\varepsilon_s + b\varepsilon_h}{a+b} \tag{3}$$

where ε_g, ε_s and ε_h are the ground emissivity, the soild emissivity and the herbaceous emissivity, respectively; *a* and *b* are the proportions of soil and herbaceous components of the pixel, respectively, which are available through some vegetation continuous field products such as MODIS MOD44.

Dimensions of the emissivity LUT for each channel include the view zenith angle, the tree cover percentage, the tree type, the soil percent cover, the herbaceous percent cover, and the LAI. As were shown in Table 1, the zenith angle was set from 0^0 to 70^0, with a 10^0 increment. It covers the MODIS view zenith angle range. The tree cover percentage range was from 10% to 90%, which implies that the background percent cover range was from 90% to 10%, with a 10% increment. Note that the background cover is composed of the soil ground and the herbaceous. Among which, the soil ground proportion range is from 0.0 to 1.0 (therefore, the herbaceous proportion is from 1.0 to 0.0) with increment 0.1. The LAI range was set from 0.2 to 5.0. Increments of the LAI were 0.2 and 1.0 for the LAI ranges from 0.2 to 1.0 and from 1.0 to 5.0, respectively. The LAI increment was set to be smaller for LAI values less than 1.0 because, according to the definition of LAI, satellite sensed radiance from a surface that is partially covered by leaves is significantly different from the radiance of a surface that is fully covered by leaves.

Three solar zenith angels were selected in the table to test if the sun-geometry will affect the directional emissivity variation. Solar-view relative azimuth is set to be 0^0 and 180^0, representing the same and opposite observation directions.

Finally, the surface temperature T_{surf} is randomly determined, within a range from 270 K to 310 K, for the calculation of the directional emissivity LUTs.

3. SIMULATION OF THE RADIATIVE TRANSFER PROCESS

3.1 Radiative transfer model

The atmospheric radiative transfer model used in this study is MODTRAN 4, version 2 reversion 1 [7]. The MODTRAN model simulates the spectral radiances from land surface received by satellite sensor through a certain atmospheric profile in a certain solar-view geometric direction. The model has been widely used in simulation studies of satellite remote sensing.

Following others [10][11][12], we simulated top of atmosphere (TOA) brightness temperatures of MODIS sensor at bands 31 and 32 using the MODTRAN code. Input parameters of the MODTRAN 4 model mainly prescribe vertical profile of atmospheric properties, the boundary surface temperature, the sensor spectral response function, the sensor view and solar (daytime only) geometry, and the surface emissivity. To determine realistic atmospheric profiles, we used the CrIS F98-Weather Products Test Bed data Package [13]. NOAA produced this set of 7547 profiles using both radiosonde and Television Infrared Observation Satellite Program (TIROS) Observational Vertical Sounder (TOVS) data. We selected 60 daytime cloud-free profiles acquired near 1000 and 1500 local time. The time is close to the equator crossing time of most solar-synchronous satellites. Only profiles with a cloud fraction index (as provided in the profile metadata) equal to zero were considered. The selected profiles spanned a latitude range from 60^0 South to 70^0 North, and a column water vapor range from 0.5 g/cm^2 to 5.6 g/cm^2.

Surface emissivity and temperature of the MODTRAN input are the values calculated from the MGP model as described above, which vary with the solar-view geometric direction. The atmospheric low boundary air temperature of each profile is adapted as the T_{surf} value in Table 1.

The MODIS sensor of AQUA satellite, band 31 and 32, spectral response functions were applied, for generating the sensor's TOA brightness temperatures at the central wavelengths around 11 μm and 12 μm, respectively.

More details of the MODTRAN simulation and the input parameter setting can also be found in [14].

3.2 Split-window LST algorithm

The LST retrieval algorithm used in this study is a path corrected split-window algorithm developed by Yu *et al*. [2], i.e.,

$$T_s = A_0 + A_1 T_{11} + A_2 (T_{11} - T_{12}) + A_3 (1 - \varepsilon) + A_4 \Delta\varepsilon + A_5 (T_{11} - T_{12})(\sec\theta - 1) \quad (4)$$

where, T_{11} and T_{12} are the TOA brightness temperatures at the two thermal infrared bands, respectively; ε and $\Delta\varepsilon$ are the mean surface emissivity and the emissivity difference between the two bands, respectively; θ is the satellite view zenith angle; A_k (k=0 to 5) are the algorithm coefficients. This is a modified version of the split-window LST algorithm used by Ulivieri *et al*. [6] and Sobrino *et al*. [15] for AVHRR LST data retrievals. Yu *et al*. [2] added to the equations a path correction term, the last term in equation (4), to correct further for directional effects of atmospheric absorption. This correction is necessary in this study because we need to exclude other directional effects as much as possible for analyzing the emissivity directional effect. The algorithm is selected because it is simple while representing those split-window LST algorithms that contain both the emissivities and emissivity difference. Coefficients of the algorithm, A_k, were derived through a regression analysis on the simulation data, as was described by Yu *et al*., [2].

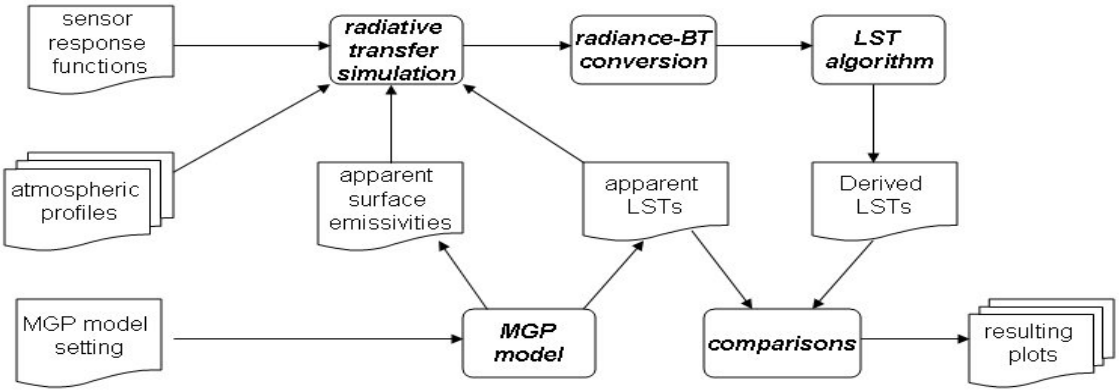

Fig. 1. Simulation processing scheme for evaluating the emissivity directional effect in LST retrieval.

For evaluating the emissivity directional effect on LST retrieval, the MODTRAN model is coupled with the MGP model. Figure 1 illustrates the simulation processing scheme. First, the MGP model settings are prepared for generating the apparent surface temperature and emissivities at the surface. Note that those temperatures and emissivities are solar-view geometric dependent. The MODTRAN simulation model takes those temperatures and emissivities, as well as the atmospheric profiles and the sensor response functions, as input values and simulates radiances (satellite sensor specific) at the top of atmosphere. The simulated radiances are then converted into the TOA brightness temperatures of the respective two thermal infrared bands. At this stage, the split-window LST algorithm is applied to calculate the satellite derived LST using the simulated brightness temperatures and the apparent emissivities.

4. SIMULATION RESULTS

4.1 MGP simulation results

Examples of the MGP model simulation are shown in Figures 2 and 3. Left panel of Figure 2 represents an example case of the MGP model parameter setting that the tree cover percentage is 30%, the LAI is 1, emissivities of the tree cover and the background for the MODIS sensor (band 31, band 32) are (0.9890, 0.9909) and (0.9450, 0.5600), respectively, and the T_{surf} is assumed to be 292 K. In the figure, the bowel-shaped solid curve represents the mean apparent emissivity seen by the satellite sensor, which increases sharply with increase of the view zenith angle. The emissivity difference between the view zenith at nadir and at the edge is about 0.014, which leads to significant differences in the retrieved LST. Also, three apparent LST curves are shown in the figure, representing three solar zenith angle settings, respectively. It is observed that, for each solar zenith angle, the apparent temperature at and near the hot spot (where view and solar zenith angles overlap) is much higher than the temperatures at other angles. The temperature difference between the ridge and off-ridge is about 2 degrees K for this particular scenario, indicating that solar reflection has

significant contribution in the total radiance budget in this direction. Note that the emissivity distribution does not change with solar zenith because emissivity of a certain surface type does not change with its sunlit or shade condition.

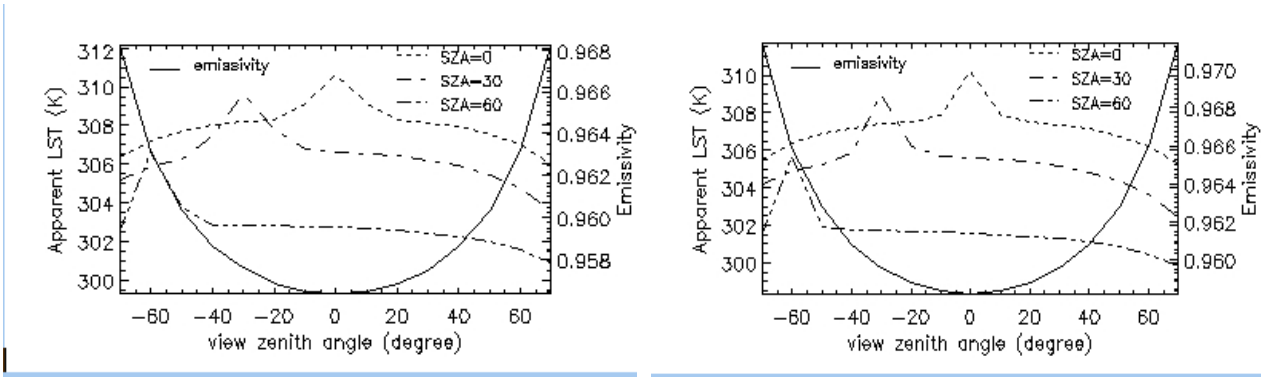

Fig. 2. Examples of the surface temperature (dash lines) and mean emissivity distribution (solid line) along with the satellite view zenith angle. LAI value is 1, vegetation coverage is 30% (left) and 60% (right).

Another example of the apparent emissivity and temperature distributions is also shown in Figure 2 (right panel), where all the parameters are the same to the left panel except that the tree cover percentage is 60%. In this panel, similar features are observed, and the emissivity difference between the view zenith at nadir and at the edge is about 0.014 also. However, it is worth to pointing out that, due to the vegetation cover increase (from 30% to 60%), the absolute value of the apparent emissivity is a little bit larger than that in the left panel. Therefore, the apparent temperature of the surface is a little bit lower than that in Figure 2. This is expected since emissivity of the vegetation in the thermal infrared band is bigger than that of the soil background.

Figure 3 further illustrates that the apparent emissivity varies with the tree cover fraction as well as the view zenith angle and the LAI. The variation is higher in the large LAI index (right panel) than that in the low LAI index (left panel). It is also shown that the emissivity variation along with the tree cover fraction and the view zenith is continuous. This is also true in the LAI dimension (not shown). The continuity feature of the directional emissivity is important for performing interpolation between the incremental dimensions, which will be applied in our MODIS data application in Section 5.

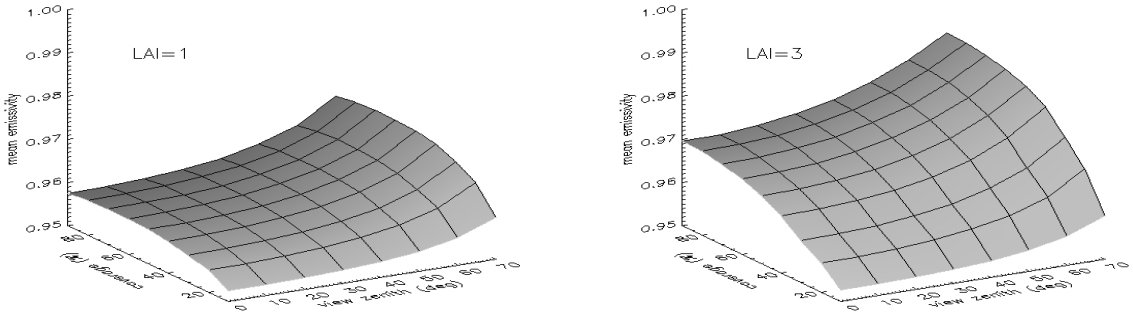

Fig. 3. Examples of the directional emissivity distributions along with the satellite view zenith angle and the vegetation coverage. LAI value is 1 (left) and 3 (right), respectively.

4.2 MODTRAN simulation results

In the MODTRAN simulation, we focused on how the LST retrieval would be impacted by the directional emissivity due to different surface tree cover fraction and LAI values. We compared the difference between the LST derived using the directional emissivity, hereafter referred to as D-LST, and the LST derived using a constant emissivity at the nadir view, hereafter referred to as LST. Figure 4 shows two examples under the atmospheric profile identified as IPR06065, which is a warm atmospheric profile with the low boundary air temperature 297 K and the total column water vapor 2.596 g/cm^2.. LAI is set to be 1, while the vegetation cover is 30% (left) and 60% (right). In the figure, it is clearly

observed that the D-LST is lower than the LST in the view zenith angles off-nadir; the larger the view zenith angle the largest the difference observed. The Figure also suggests that the differences are almost identity in different solar zenith angles. Note that maximum difference between the D-LST and the LST is increased a little bit in the right panel, because the emissivity of the vegetation component is bigger than that of the soil ground component.

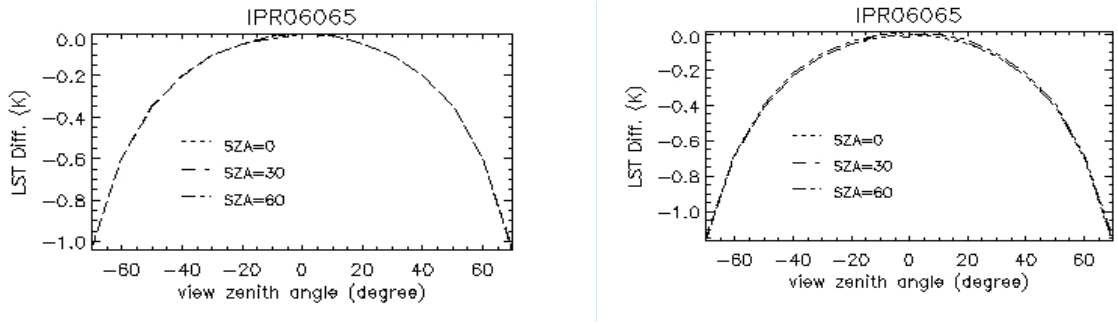

Fig. 4. Example plots of the LST retrieval difference between using the directional emissivities and using a constant emissivity. The temperature and emissivity distributions are calculated from the MGP model with the table 1 settings, for solar zenith angle at 0, 30 and 60 degrees, respectively; the LAI value is 1 and the vegetation coverage is 30% (left) and 60% (right).

In Figure 5, we plotted all the retrieved D-LSTs and the LSTs using all the atmospheric profiles and all the tree cover fraction and the LAI combinations. The low boundary temperature range of the atmospheric profiles is approximately between 270 K to 315 K. Differences between the D-LST and LST are shown in the scattered plots away from the diagonal line. Because the plots include all the view zenith data, it shows a continuity distribution in all the temperature range. The plots scattered most away from the diagonal line represent the data with the largest view zenith angles. The maximum D-SLT and the LST difference in all the results is about 1.45 K, meaning that an error budget up to 1.45 K due to the emissivity directional effect could be corrected.

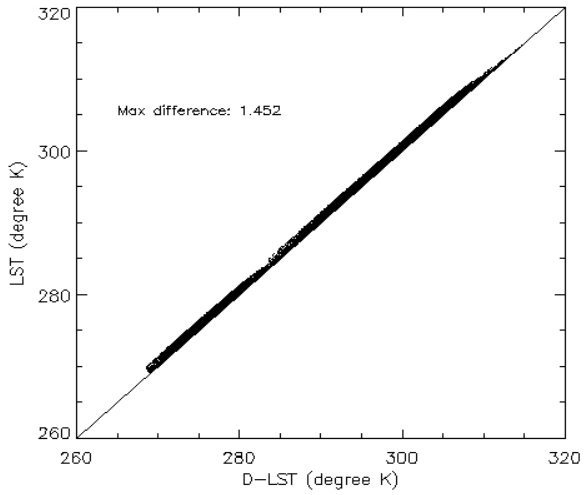

Fig. 5. The LST retrieval difference over all the simulation data.

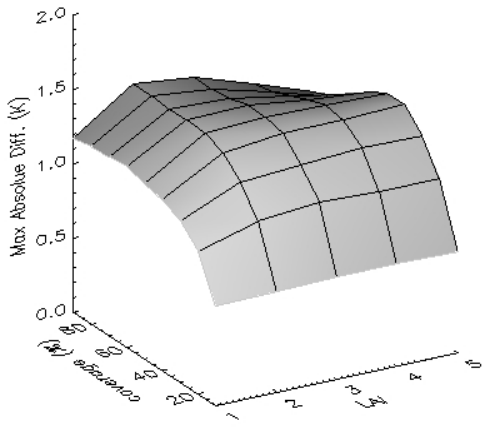

Fig. 6. Distribution of the maximum LST retrieval difference.

To further understand the LST difference corresponding to the tree cover fraction and the LAI, in Figure 6 we present a 3-D LST difference distribution for those parameters. The maximum LST difference is defined as the data from the simulation results of all the atmospheric profiles with certain tree cover fraction and the LAI. The Figure shows that the maximum LST difference is dominated by the tree cover fraction. This is particularly true when the LAI is less than 2. Note that the maximum LST difference changes sharply for tree cover fractions lower than 50%. For greater fractions, changes of the LST difference are rather small.

5. MODIS DATA APPLICATION

We further estimate the directional effect in actual MODIS LST data. The MODIS LST swath product was derived using a generalized split-window algorithm, in which the surface emissivity value was primarily obtained from the surface classification maps. In other words, it used a constant emissivity value for all the view zenith direction. We therefore expect that there would be errors involved due to the directional effect.

Four MODIS swaths (5-minute scene) were used from the Aqua satellite and collected in March, 2004. Considering that the LST directional effect will mostly occur over vegetation structured surface, we selected MODIS scenes covering the north-east of the United States where trees are prevalent.

Several MODIS products and ancillary data were needed for deriving the D-LST. First, the MODIS radiance data (MOD02) was used to determine the TOA brightness temperatures. The cloud mask data (MOD35) was used for filtering the cloudy data, where only the "confident cloud-free" (a cloud mask index value) pixels were left for further processing. For estimating the directional emissivity, we collected the vegetation continuity fields (VCF) and the LAI data [16]. The VCF is an accumulated annual data set and was estimated in year 2002; we assumed that its values over north-east of the United States are still accurate The VCF data provide probabilities of tree cover, soil cover and herbaceous cover for a ground area. The LAI data includes a monthly mean product available since February, 2000. Both the VCF and LAI datasets are 0.5 km ground resolution and are in the integerized sinusoidal projection. Finally, the MODIS geometry data (MOD03) was used for projecting the VCF and LAI data onto the swath latitudes and longitudes. There were four tree cover types in the VCF data: green needle forest, green broadleaf forest, senescent needle forest and senescent broadleaf forest. The pixels that only contain tree cover were used in this study. The VCF data also provide two ground types: soil and herbaceous. Emissivity of the background is calculated using equation [3].

The directional emissivities of the MODIS bands 31 and 32 were estimated from the lookup tables (LUTs) generated through the MGP model simulation described in Section 2. One LUT represents a tree type and a band. Dimensions of the LUT include view zenith, tree cover fraction, soil cover fraction and the LAI. The nadir view emissivity values of each tree type and background type were estimated from Snyder *et al*.' classes [3]. Incremental values of the corresponding dimensions were shown in Table 1. In the processing, we first obtained the view zenith and the latitude/longitude information of the pixel from the MOD03 dataset. We then projected the pixel location for obtaining the tree cover percentage and the soil cover fraction as well as the tree type information from the VCF dataset, and the LAI value from the LAI dataset. Finally, a bi-linear multi-dimension interpolation process was performed to calculate the directional emssivities from the LUTs.

The D-LST was calculated using split-window LST algorithm (Eq.4) with the directional emissivities and the TOA radiance data. We then compared with the MODIS LST product. Note that the MODIS VCF and the LAI data are experimental products; the quality of the products is not fully studied. Errors in the VCF and the LAI data will be transferred to the D-LST and such errors are hard to estimate, and as a result, comparisons between the D-LST and MODIS LST for individual pixels are less meaningful. However, if we consider large areas the D-LST errors due to the errors of VCF and LAI data are in a certain distribution, then a statistically meaningful comparison between the D-LST and the MODIS LST is possible. In this study we compared the D-LST and the MODIS LST using histogram plots over 549,240 pixels collected from the four MODIS scenes.

Figure 7 shows the comparison results. To better illustrate the emissivity directional effect in the MODIS LST product, we plotted the histograms of the D-LST and the MODIS LST difference in three view zenith angle ranges (top three panels), as well as in a total view zenith range (bottom panel). Looking at the top panel of Figure 10, which represents the results for the view zenith angle range from 0^0 to 20^0 degree, the difference of D-LST and the MODIS LST is primarily a normal distribution biased negatively. The normal distribution difference and the bias can be explained by the fact that since the two LSTs were produced independently from different algorithms and, in each algorithm, there were a variety of error sources. However, it is observed that the tail part at the negative direction is longer than that in the positive direction. This negatively biased tail feature is getting more and more obvious in the view zenith angle range from 20^0 to 45^0 (upper-middle panel) and in the range from 45^0 to 65^0, indicating that more and more D-LSTs were negatively biased comparing to the MODIS LST as the view zenith angle increased. The standard deviation of the D-LST and the MODIS LST difference is therefore increased when the view zenith increased. This supports the results obtained with our simulation studies.

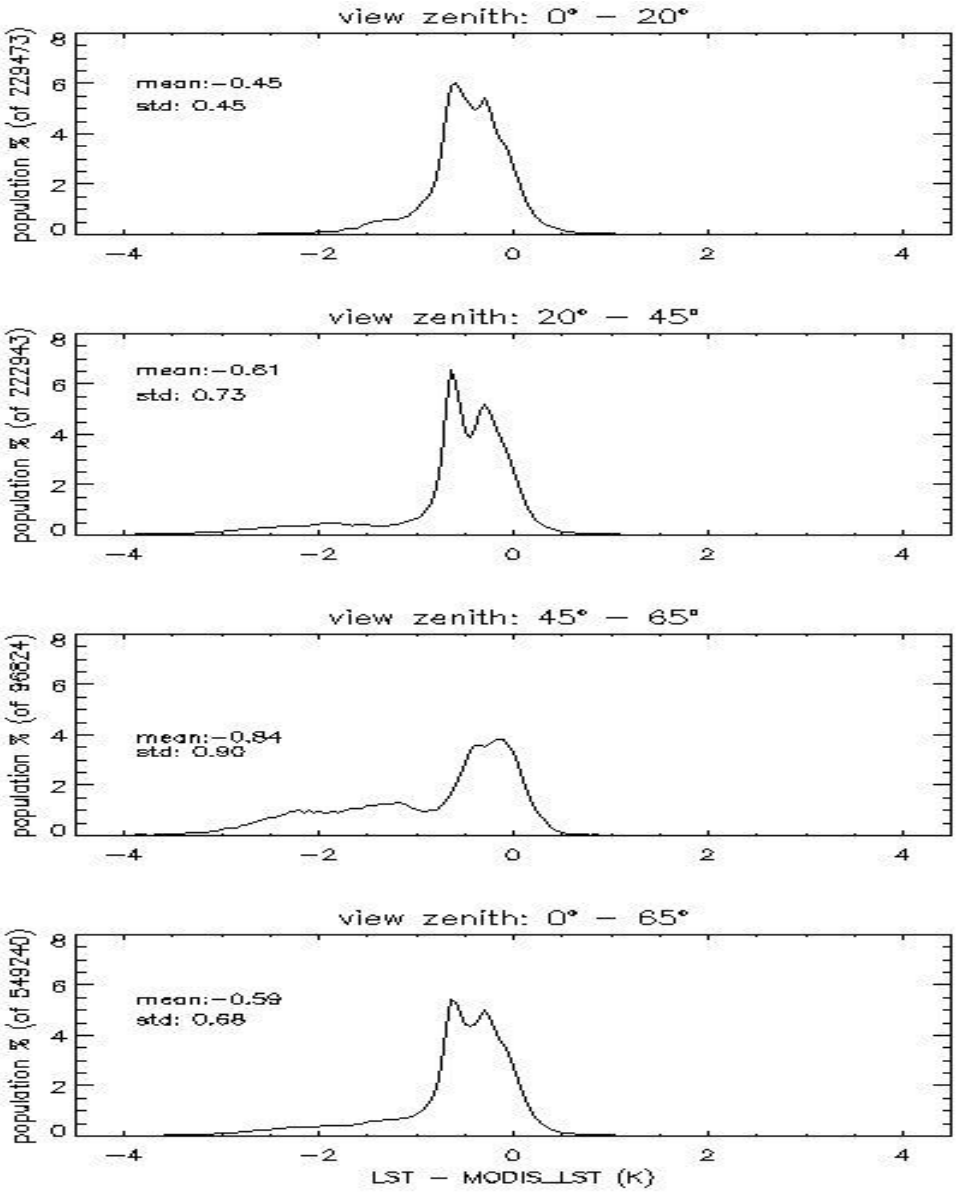

Fig.7. Histogram plots of LST difference between the D-LST and the MODIS LST (MOD11). The statistics was calculated from 4 scenes of MODIS 5-minute swath data in March, 2004, north-east of the United States.

6. DISCUSSION

The MGP model simulation results demonstrated that a structured vegetation surface may have considerable emissivity variation along with the satellite sensor view zenith angle (Figure 2), the vegetation and the background types, the vegetation LAI, and the tree cover fraction. The view zenith dependency, which is the focus of this study, results from the variation of the satellite viewed surface components with the view zenith due to the surface structure. The emissivity directional variation is a secant-like distribution to the view zenith angle, which implies that the emission property of the composed surface is dominated by the projected viewing area of the vegetation surface. Large values of LAI will also increase its projected view area and therefore will increase considerably the emissivity directional variability. This is observed through Figure 3. It is obvious that the directional emissivity varies with the tree cover fraction due to the increase of the high emission component.

It is important to note that the directional emissivity variation does not change with the solar angle, because the emission property of a surface component is independent of its temperature, and therefore sunlit and shaded elements have the same emissivity.

The directional emissivity variation directly affects the LST retrieval. In the MODTRAN simulation, we observed that the D-LST is less than the LST at the off nadir views (Figures 5 and 6). The difference between the D-LST and the LST may be considerably large when the view zenith is larger than 40^0, and can exceed 1.4 K at the edge. It is likely a reversed secant distribution along with the view zenith angle. It may have a large impact on retrieving the LST from cross-scan satellite sensors. For instance, about 40% LST data retrieved using MODIS sensor, which measures the surface in a view zenith range from 0^0 to 65^0, may be significantly overestimated.

Note again that the differences are almost the same for different solar zenith angles, which verifies that surface emission property does not change with the sunlit. It is also interesting to note that, although there is a temperature ridge occurring at the solar reflect angle in the surface temperature directional distribution, the temperature difference between the D-LST and the LST is not affected by the solar reflectance. The split-window LST algorithm detected the temperature ridge by the TOA brightness temperatures and the difference of the brightness temperatures.

Our MODIS data application indicates that there is a tail structure coupled on the normal-like distribution of the histogram of the D-LST and the LST difference. Assuming that the normal-like distribution was introduced because of the algorithm difference and the data noise, Figure 7 demonstrates the emissivity directional effect in the LST retrieval: the retrieved LST with a directionally independent emissivity may be overestimated in the off nadir view zenith angles.

There are two ways to correct the directional effect. As is shown in the MODIS data application, we used the LUTs of the directional emissivity to replace the constant emissivity in the LST algorithm. In this method, the LUTs are based on the MGP model, while the LUT indices are calculated at runtime using the ancillary data such as the VCF data and the LAI data.

Alternatively, the D-LST can be obtained by adding a directional correcting amount, ΔT_s, to the traditional LST. The directional correcting amount can be a LUT generated by coupling the MGP model and the MODTRAN radiative transfer model. In this study we calculated the LUT and applied it to the MODIS data. Comparison results (shown here) between the directional effect corrected LST using the ΔT_s LUT and the MODIS LST are pretty much the same as figure 7.

7. CONCLUSION

We simulated the impacts of structural directional emissivity on LST retrievals. We developed a methodology (based on a LUT) to correct for those effects by using the MGP model coupled to the MODTRAN model. We apply our method to MODIS scenes and show that, for structured vegetation surface, the emissivity of a land surface pixel may be considerably different for different observation angles. The directional variation of the surface emissivity therefore may introduce error in the LST retrieval when most split-window algorithms are used. For the scenarios studied in this work, the maximum LST error introduced by the emissivity directional effect may exceed 1.4 K, which is significant for many LST applications.

We presented a method for correcting the emissivity directional effect using a LUTs. The dimension indices of the LUTs can be determined using the current MODIS data and its ancillary data. Applying the method on MODIS data, we revealed the possible LST error of the directional effect in the MODIS LST data.

The LST error of the emissivity directional effect is considerably large when the view zenith is larger than 40^0. In the MODIS case it means that about 40% of the MODIS LST data may be significantly overestimated. We proposed a method to correct the error using a pre-calculated LUT. Further studies are needed to apply the method to MODIS data.

REFERENCES

1. G. A. Maul and M. Sidran, "Atmospheric effects on ocean surface temperature sensing from NOAA satellite scanning radiometer", *J. Geophys. Res.*, 78, pp 1909-1916, 1973.

2. Y. Yu, J. L. Privette and A. C. Pinheiro, "Evaluation of split window land surface temperature algorithms for generating climate data records", *Proceed. of The 9th International Symposium on Physical Measurements and Signatures in remote Sensing*, pp 115-118, 2005.
3. W. C. Snyder, Z. Wan and Y. Z. Feng, "Classification-based emissivity for land surface temperature measurement from space". *Int. J. Remote Sensing*, vol. 19, no. 14, pp. 2753-2774, 1998.
4. Z. Wan and Z.-L. Li, "A physics-based algorithm for retrieving land surface emissivity and temperature from EOS/MODIS data", *IEEE Trans. Geosci. Remote Sensing*, vol. 35, pp. 980–996, 1997.
5. A. C. Pinheiro, J. L. Privette, R. Mahoney and C. J. Tucker, "Directional effects in a daily AVHRR land surface dataset over Africa", *IEEE Trans. Geosci. Remote Sensing*, vol. 42 pp. 1941-1954, 2004.
6. C. Ulivieri, M.M. Castronouvo, R. Francioni and A. Cadillo, "A SW algorithm for estimating land surface temperature from satellites" , *Adv. Spce res*., 14, 3, 59-65, 1992.
7. A. Berk, G. P. Anderson, P. K. Acharya, J. H. Chetwynd, M. L. Hoke, L. S. Bernstein, E.P. Shettle, M.W. Matthew and S.M. Alder-Golden , *MODTRAN4 Version 2 Users's Manual*, Space Vehicles Directorate, Hanscom AFB, MA 01731-3010, April 2000.
8. W. Ni, X. Li, C. E. Woodcock, M. R. Caetano and A. H. Strahler, "An analytical hybrid GORT model for bidirectional reflectance over discontinuous canopies", *IEEE Trans. Geosci. Remote Sensing*, vol. 37, pp. 987-999, 1999.
9. A. C. Pinheiro, J. L. Privette, and P. Guillevic, "Modeling the observed angular anisotropy of land surface temperature in a savanna, *IEEE Trans. Geosci. Remote Sensing*, vol. 44(4), pp. 1036-1047, 2006.
10. Z. Wan, and J. Dozier, "A generalized split-window algorithm for retrieving land-surface temperature measurement from space*", IEEE Trans. Geosci. Remote Sensing*, vol. 34, pp. 892–905, 1996.
11. J. Ip, Operational Algorithm Description Document for the VIIRS Land Surface Temperature (LST) EDR Software, Northrop Grumman Space Technology, Redondo Beach, CA 90278. Doc. D38714, June 2004.
12. H. Ouaidrari, S.N. Goward, K.P. Czajkowski, JA Sobrino and E Vermote, "Land surface temperature estimation from AVHRR thermal infrared measurements: An assessment for the AVHRR Land Pathfinder II data set*, Remote Sensing of Environment*, vol. 81, no**.** 1, pp. 114-228, 2002.
13. NOAA88, The CrIS F98-Weather Products Test Bed Data Package, NOAA88, Rev. 1.0, M. Goldberg, personal communication, 1998.
14. Y. Yu, J. L. Privette and A. C. Pinheiro, "Analysis of the NPOESS VIIRS land surface temperature algorithm using MODIS data", *IEEE Trans. Geosci. Remote Sensing*, vol. 43, no. 10, pp. 2340-2350, 2005.
15. J.A. Sobrino, Z.L. Li, M.Ph. Stoll, F. Becker, "Improvements in the split-window technique for land surface temperature determination", *IEEE Trans. Geosc. Remote Sens*., 32, 2, 243-253, 1994.
16. Boston University, Climate and Vegetation Research Group, http://cybele.bu.edu/modismisr/index.html